Journal of Solid State Chemistry **154,** 514–523 (2000)
doi:10.1006/jssc.2000.8872, available online at http://www.idealibrary.com on IDEAL®

Hydrothermal Synthesis and Characterization of Two Mixed Valence Piperazine–Vanadium Phosphates: $(C_4H_{12}N_2)(H_3O)[(VOPO_4)_4(H_2O)H_2PO_4]\cdot 3H_2O$ and $(C_4H_{12}N_2)[(VO)(VO_2)_2(H_2O)(PO_4)_2]$

Junghwan Do, Ranko P. Bontchev, and Allan J. Jacobson[1]

Department of Chemistry, University of Houston,Houston, Texas 77204–5641

Received May 2, 2000; in revised form June 19, 2000; accepted July 13, 2000; published online September 30, 2000

Two new phases, $(C_4H_{12}N_2)(H_3O)[(VOPO_4)_4(H_2O)H_2PO_4]\cdot 3H_2O$ (1) and $(C_4H_{12}N_2)[(VO)(VO_2)_2(H_2O)(PO_4)_2]$ (2) have been synthesized hydrothermally and characterized by single crystal X-ray diffraction, thermogravimetric analysis, and magnetic susceptibility. Compound 1 has an open-framework structure and is closely related to $(VO)_2(PO_4)_2H_2PO_4\cdot N_2C_2H_{10}$, whereas compound 2 has layered structure containing discrete trinuclear $[V_3O_{13}(H_2O)]$ corner-sharing units. In both structures the V atoms are mixed-valence, V^{IV} and V^{V}, with octahedral and trigonal bipyramidal geometry. Crystal data: $(C_4H_{12}N_2)(H_3O)[(VOPO_4)_4(H_2O)H_2PO_4]\cdot 3H_2O$ 1, monoclinic, space group $P2/n$ (No. 13), a =9.6448(7) Å, b = 8.8770(7) Å, c = 14.813(1) Å, β = 91.936(2)°, Z = 4, $R1$ = 0.0717; $(C_4H_{12}N_2)[(VO)(VO_2)_2(H_2O)(PO_4)_2]$ 2, triclinic, space group $P\bar{1}$ (No. 2); a = 6.1650(5) Å, b = 10.8206(9) Å, c = 11.854(1) Å, α = 66.598(1)°, β = 76.008(2)°, γ = 83.439(2)°, Z = 2, $R1$ = 0.0467.

Key Words: **hydrothermal synthesis; piperazine; vanadium phosphate; mixed valence.**

INTRODUCTION

Vanadium phosphate phases have been intensively studied due to the wide diversity of their structural chemistry and because of their potential applications in catalysis, adsorption, and ion exchange (1–4). A large number of vanadium phosphates incorporating organic species such as monoammonium and diammonium cations are known. Depending on the charge, shape, and size of the organic cation, structures with rings/cages, cavities, or layers are formed (5). Several vanadium phosphates containing diprotonated piperazine (pipz-VPOs) have been previously reported. Examples include layered structures closely related to the structure of α-$VOPO_4\cdot 2H_2O$ and framework structures with tunnels occupied by diprotonated piperazine cations (6–10).

In this paper, we report the hydrothermal synthesis and characterization of the first examples of mixed-valence pipz-VPO compounds. Compound **1** $(C_4H_{12}N_2)(H_3O)[(VOPO_4)_4(H_2O)H_2PO_4]\cdot 3H_2O$ has a framework structure based on the α-$VOPO_4\cdot 2H_2O$ structure and $(C_4H_{12}N_2)[(VO)(VO_2)_2(H_2O)(PO_4)_2]$ **2** is a layered compound that contains a unique trinuclear arrangement of vanadium cations.

EXPERIMENTAL

Synthesis of $(C_4H_{12}N_2)(H_3O)[(VOPO_4)_4(H_2O)H_2PO_4]\cdot 3H_2O$ (1)

The reactants V_2O_3 (0.0525 g, 0.35 mmol), H_3BO_3 (0.0868 g, 1.0 mmol), H_3PO_4 (0.096 mL, 85 wt% solution in H_2O, 1.37 mmol), piperazine (0.0151 g, 0.025 mmol), and Na_2CO_3 (0.0093 g, 0.09 mmol) were added to 2 mL (166 mmol) water. The initial pH was 2.94. The reaction was carried out in a 23-mL capacity Teflon-lined stainless steel Parr hydrothermal bomb. The starting materials were heated at 145°C for 3 days. Afterward, the reactor was cooled to room temperature over a 1-day period (final pH 3.12). The product was recovered by vacuum filtration and washed with distilled water. Dark green rod-shaped crystals ($\sim$30% yield based on V) were obtained together with a second phase identified as the known phase $[VO(H_2O)_3][VO(H_2O)](VO)_2(PO_4)_2(HPO_4)_2$ $(C_4H_8N_2H_4)$ (10). The crystals of **1** were stable in water and in air. Subsequently, **1** was prepared under the same reaction conditions but omitting the H_3BO_3 and Na_2CO_3.

Synthesis of $(C_4H_{12}N_2)[(VO)(VO_2)_2(H_2O)(PO_4)_2]$ (2)

The compound was synthesized by a two-step reaction. In the first step, V_2O_5 (9.094 g, 0.05 mol) was slowly added to

[1]To whom correspondence should be addressed. Fax: (713) 743-2787. E-mail: ajjacob@uh.edu.

0022-4596/00 $35.00

a mixture of oxalic acid (4.502 g, 0.05 mol), H_3PO_4 (13.65 mL, 85 wt% solution in H_2O, 0.2 mol), and 250 mL distilled water at 70°C. The blue solution was boiled overnight in a 500-mL flask. At this point no crystallization had occurred. The resulting blue solution (solution A) was used as a reagent in the second step of the synthesis. A mixture of solution A (10 mL: V, 3.7 mmol; P, 7.4 mmol), H_3BO_3 (0.155 g, 2.5 mmol), and piperazine (0.108 g, 1.25 mmol) was heated at 145°C for 4 days in a Parr hydrothermal reactor. The initial pH was 2.12. Afterward, the reactor was cooled to room temperature over a 1-day period (final pH 1.74). The product was washed with water and brown plate-shaped crystals ($\sim$ 42% yield based on V) were obtained together with unidentified pale green powder.

Characterization

The crystal structures of **1** and **2** were determined by single-crystal X-ray diffraction methods. Preliminary examination and data collection were performed on a SMART platform diffractometer equipped with 1 K CCD area detector using graphite-monochromatized Mo$K\alpha$ radiation at

TABLE 1
Crystallographic Data for 1 and 2

	1	**2**
Empirical formula	$C_4H_{25}N_2O_{29}P_5V_4$	$C_4H_{14}N_2O_{14}P_2V_3$
Formula weight, amu	923.68	528.93
Space group	$P2/n$ (No. 13)	$P\bar{1}$ (No. 2)
a (Å)	9.6448(7)	6.1650(5)
b (Å)	8.8770(7)	10.8206(9)
c (Å)	14.813(1)	11.854(1)
α (deg.)	90	66.598(1)
β (deg.)	91.936(2)	76.008(2)
γ (deg.)	90	83.439(2)
V (Å^3)	1267.5(2)	704.0(1)
Z	4	2
T (K)	297(2)	297(2)
λ (Å)	0.71073	0.71073
μ (mm^{-1})	1.876	2.264
ρ (calc.) (g cm^{-3})	2.392	2.495
Crystal size (mm^3)	$0.20 \times 0.04 \times 0.04$	$0.10 \times 0.06 \times 0.02$
No. of unique reflections	2231	2992
No. of parameters	197	228
Goodness-of-fit on F^2	1.195	1.100
R_1 [$I > 2\sigma(I)$][a]	0.0717	0.0467
wR_2 (all data)	0.1497[b]	0.0996[c]
$(\Delta\rho)_{max}$; $(\Delta\rho)_{min}$ (e/Å^3)	1.707; $-$0.910	0.618; $-$0.600

[a] $R_1 = \sum||F_o| - |F_c|/\sum|F_o|$.

[b] $wR_2 = [\sum w(|F_o| - |F_c|)^2/\sum w|F_o|2]^{1/2}$; $w = 1/[\sigma^2(F_o^2) + (0.0010)^2 + 24.33P]$; $P = [\mathrm{Max}(F_o^2, 0) + 2F_c^2]/3$.

[c] $R_w = [\sum w(|F_o| - |F_c|)^2/\sum w|F_o|2]^{1/2}$; $w = 1/[\sigma^2(F_o^2) + (0.0129P)^2 + 4.47P]$; $P = [\mathrm{Max}(F_o^2,0) + 2F_c^2]/3$ (all data).

TABLE 2
Atomic Coordinates ($\times 10^4$) and Equivalent Isotropic Displacement Parameters (Å$^2 \times 10^3$) for 1 and 2

	x	y	z	U_{eq}[a]
		1		
V(1)	9355(1)	$-$ 21(2)	1513(1)	6(1)
V(2)	11685(2)	$-$ 5002(2)	$-$ 1068(1)	20(1)
P(1)	10080(2)	$-$ 2527(2)	47(1)	8(1)
P(2)	7500	2531(3)	2500	8(1)
P(3)	7500	$-$ 2477(3)	2500	9(1)
P(4)	12500	1046(4)	2500	12(1)
O(1)	10469(5)	$-$ 1617(6)	882(4)	12(1)
O(2)	11357(6)	$-$ 3504(6)	$-$ 167(4)	15(1)
O(3)	10349(5)	1573(6)	778(4)	11(1)
O(4)	8818(5)	$-$ 1545(6)	2437(4)	12(1)
O(5)	8803(6)	1607(6)	2383(4)	14(1)
O(6)	12710(6)	$-$ 6502(6)	$-$ 1654(4)	16(1)
O(7)	12797(6)	$-$ 3552(6)	$-$ 1662(4)	14(1)
O(8)	11186(6)	$-$ 6439(6)	$-$ 198(4)	14(1)
O(9)	7976(5)	$-$ 93(7)	885(4)	17(1)
O(10)	10296(6)	$-$ 4933(8)	$-$ 1668(4)	27(2)
O(11)	11214(5)	110(6)	2401(3)	10(1)
O(12)	12594(6)	2114(7)	1659(4)	22(1)
O(13)	13856(12)	$-$ 5100(15)	$-$ 246(8)	31(4)
N	5129(7)	215(9)	938(4)	19(2)
C(1)	4413(9)	$-$ 1139(11)	581(6)	22(2)
C(2)	4991(10)	1525(11)	332(6)	25(2)
OW1	2500	7066(17)	2500	93(5)
OW2	4157(18)	4850(17)	1562(10)	56(6)
OW3	3362(29)	5226(26)	1119(17)	78(11)
		2		
V(1)	2644(1)	6941(1)	3909(1)	9(1)
V(2)	7990(1)	7488(1)	8717(1)	10(1)
V(3)	4781(1)	4079(1)	8242(1)	10(1)
P(1)	3021(2)	6393(1)	9368(1)	9(1)
P(2)	2172(2)	4009(1)	6268(1)	9(1)
O(1)	6013(6)	5336(3)	7061(3)	19(1)
O(2)	1626(5)	5446(3)	5419(3)	12(1)
O(3)	$-$ 337(5)	6948(3)	3560(3)	13(1)
O(4)	9326(6)	6318(4)	7660(3)	19(1)
O(5)	2169(5)	3988(3)	7580(3)	14(1)
O(6)	2815(5)	5021(3)	9322(3)	15(1)
O(7)	5207(5)	7076(3)	8445(3)	13(1)
O(8)	5603(5)	6503(3)	4310(3)	13(1)
O(9)	3815(5)	7380(3)	2339(3)	12(1)
O(10)	11086(5)	7335(3)	8895(3)	16(1)
O(11)	6871(5)	7637(3)	10083(3)	12(1)
O(12)	7024(5)	3694(3)	9313(3)	14(1)
O(13)	2249(5)	8287(3)	4205(3)	16(1)
O(14)	8165(6)	9006(3)	7690(3)	18(1)
N(1)	9719(7)	11354(4)	9128(4)	16(1)
N(2)	14686(9)	8617(5)	5864(5)	35(1)
C(1)	7740(8)	10503(5)	9928(5)	19(1)
C(2)	11689(9)	10512(5)	8860(4)	18(1)
C(3)	16913(10)	9094(7)	5034(6)	36(1)
C(4)	13401(10)	9735(7)	6150(5)	37(2)

[a] U_{eq} is defined as one-third of the trace of the orthogonalized U_{ij} tensor.

TABLE 3
Selected Bond Lengths (Å) and Angles (°) for 1 and 2

	1[a]		
V(1)–O(9)	1.599(5)	V(2)–O(10)	1.583(6)
V(1)–O(4)	2.004(6)	V(2)–O(6)	1.887(6)
V(1)–O(5)	2.019(6)	V(2)–O(8)	1.888(6)
V(1)–O(1)	2.026(6)	V(2)–O(7)	1.907(6)
V(1)–O(3)	2.045(6)	V(2)–O(2)	1.917(6)
V(1)–O(11)	2.191(5)	V(2)–O(13)	2.39(1)
P(1)–O(1)	1.513(6)	P(2)–O(5)^{3}	1.514(6)
P(1)–O(3)^{1}	1.531(6)	P(2)–O(5)	1.514(6)
P(1)–O(2)	1.550(6)	P(2)–O(7)^{1}	1.558(6)
P(1)–O(8)^{2}	1.550(6)	P(2)–O(7)^{4}	1.558(6)
P(3)–O(4)	1.521(6)	P(4)–O(11)	1.496(5)
P(3)–O(4)^{3}	1.521(6)	P(4)–O(11)^{6}	1.496(5)
P(3)–O(6)^{2}	1.555(6)	P(4)–O(12)^{6}	1.573(6)
P(3)–O(6)^{5}	1.555(6)	P(4)–O(12)	1.573(6)
N–C(2)	1.47(1)	N–C(1)	1.48(1)
C(1)–C(2)^{7}	1.53(1)	C(2)–C(1)^{7}	1.53(1)
N–H0A···O(5)	2.934(9)	N–H0A···O(11)	2.819(8)
N–H0A···O(9)	2.764(9)		
O(4)–V(1)–O(5)	88.1(2)	O(6)–V(2)–O(8)	89.2(3)
O(4)–V(1)–O(1)	89.8(2)	O(6)–V(2)–O(7)	87.3(2)
O(5)–V(1)–O(3)	89.0(2)	O(8)–V(2)–O(2)	86.7(2)
O(1)–V(1)–O(3)	88.4(2)	O(7)–V(2)–O(2)	87.8(3)
O(9)–V(1)–O(11)	178.5(3)	O(10)–V(2)–O(13)	176.5(4)
O(1)–P(1)–O(3)^{1}	114.2(3)	O(5)^{3}–P(2)–O(5)	114.5(5)
O(1)–P(1)–O(2)	106.8(3)	O(5)^{3}–P(2)–O(7)^{1}	106.0(3)
O(3)^{1}–P(1)–O(2)	109.9(3)	O(5)–P(2)–O(7)^{1}	110.8(3)
O(1)–P(1)–O(8)^{2}	111.9(3)	O(5)^{3}–P(2)–O(7)^{4}	110.8(3)
O(3)^{1}–P(1)–O(8)^{2}	104.4(3)	O(5)–P(2)–O(7)^{4}	106.0(3)
O(2)–P(1)–O(8)^{2}	109.5(3)	O(7)^{1}–P(2)–O(7)^{4}	108.7(5)
O(4)–P(3)–O(4)^{3}	114.2(5)	O(11)–P(4)–O(11)^{6}	112.5(5)
O(4)–P(3)–O(6)^{2}	110.7(3)	O(11)–P(4)–O(12)^{6}	110.0(3)
O(4)^{3}–P(3)–O(6)^{2}	106.3(3)	O(11)^{6}–P(4)–O(12)^{6}	109.1(3)
O(4)–P(3)–O(6)^{5}	106.3(3)	O(11)–P(4)–O(12)	109.1(3)
O(4)^{3}–P(3)–O(6)^{5}	110.7(3)	O(11)^{6}–P(4)–O(12)	110.0(3)
O(6)^{2}–P(3)–O(6)^{5}	108.7(5)	O(12)^{6}–P(4)–O(12)	105.8(5)
N–H0A···O(5)	121	N–H0A···O(11)	156
N–H0A···O(9)	162		
	2[b]		
V(1)–O(13)	1.609(3)	V(2)–O(14)	1.606(3)
V(1)–O(9)	1.714(3)	V(2)–O(11)	1.663(3)
V(1)–O(2)	1.899(3)	V(2)–O(7)	1.950(3)
V(1)–O(8)	1.955(3)	V(2)–O(10)	1.952(3)
V(1)–O(3)	1.977(3)	V(2)–O(4)	2.091(3)
V(3)–O(1)	1.610(3)	V(3)–O(5)	1.982(3)
V(3)–O(9)^{1}	1.995(3)	V(3)–O(12)	1.999(3)
V(3)–O(6)	2.038(3)	V(3)–O(11)^{2}	2.226(3)
P(1)–O(12)^{2}	1.521(3)	P(2)–O(8)^{1}	1.527(3)
P(1)–O(6)	1.527(3)	P(2)–O(2)	1.531(3)
P(1)–O(10)^{3}	1.539(3)	P(2)–O(3)^{4}	1.543(3)
P(1)–O(7)	1.559(3)	P(2)–O(5)	1.546(3)
N(1)–C(2)	1.482(6)	C(1)–C(2)^{6}	1.516(7)
N(1)–C(1)	1.496(6)	C(2)–C(1)^{6}	1.516(7)
N(2)–C(4)	1.477(8)	C(3)–C(4)^{7}	1.508(9)
N(2)–C(3)	1.492(8)	C(4)–C(3)^{7}	1.508(9)
N(1)–H1A···O(3)	2.932(5)	N(1)–H1A···O(9)	2.984(5)
N(1)–H1B···O(12)	2.919(5)	N(1)–H1B···O(11)	2.961(5)
N(2)–H2A···.O(13)	2.892(6)	N(2)–H2B···O(7)	2.922(6)
O(13)–V(1)–O(9)	108.4(2)	O(13)–V(1)–O(2)	108.8(2)
O(9)–V(1)–O(2)	142.8(2)	O(13)–V(1)–O(8)	95.7(2)
O(9)–V(1)–O(8)	90.5(1)	O(2)–V(1)–O(8)	86.22(13)
O(13)–V(1)–O(3)	96.5(2)	O(9)–V(1)–O(3)	89.7(1)
O(2)–V(1)–O(3)	85.7(1)	O(8)–V(1)–O(3)	166.97(14)
O(14)–V(2)-O(11)	104.9(2)	O(14)–V(2)–O(7)	96.4(2)
O(11)–V(2)–O(7)	95.91(14)	O(14)–V(2)–O(10)	95.6(2)
O(11)–V(2)–O(10)	95.9(2)	O(7)–V(2)–O(10)	160.39(14)
O(14)–V(2)–O(4)	103.9(2)	O(11)–V(2)–O(4)	151.2(2)
O(7)–V(2)–O(4)	81.51(13)	O(10)–V(2)–O(4)	80.59(14)
O(5)–V(3)–O(9)^{1}	87.01(13)	O(9)^{1}–V(3)–O(12)	89.39(13)
(5)–V(3)–O(6)	89.49(13)	O(12)–V(3)–O(6)	88.54(13)
O(1)–V(3)–O(11)^{2}	178.0(2)		
O(12)^{2}–P(1)–O(6)	112.8(2)	O(12)^{2}–P(1)–O(10)^{3}	108.0(2)
O(6)–P(1)–O(10)^{3}	109.9(2)	O(12)^{2}–P(1)–O(7)	110.2(2)
O(6)–P(1)–O(7)	109.7(2)	O(10)^{3}–P(1)–O(7)	105.9(2)
O(8)^{1}–P(2)–O(2)	111.3(2)	O(8)^{1}–P(2)–O(3)^{4}	107.7(2)
O(2)–P(2)–O(3)^{4}	109.7(2)	O(8)^{1}–P(2)–O(5)	111.8(2)
(2)–P(2)–O(5)	108.6(2)	O(3)^{4}–P(2)–O(5)	107.6(2)
N(1)-H1A···O(3)	150	N(1)–H1A···O(9)	135
N(1)–H1B···O(12)	105	N(1)–H1B···O(11)	137
N(2)–H2A···O(13)	160	N(2)–H0A···O(7)	156

[a] Symmetry transformations used to generate equivalent atoms: 1, $-x+2, -y, -z$; 2, $-x+2, -y-1, -z$; 3, $-x+\frac{3}{2}, y, -z+\frac{1}{2}$; 4, $x-\frac{1}{2}, -y, z+\frac{1}{2}$; 5, $x-\frac{1}{2}, -y-1, z+\frac{1}{2}$; 6, $-x+\frac{5}{2}, y, -z+\frac{1}{2}$; 7, $-x+1, -y, -z$

[b] Symmetry transformations used to generate equivalent atoms: 1, $-x+1, -y+1, -z+1$; 2, $-x+1, -y+1, -z+2$; 3, $-x-1, y, z$; 4, $-x, -y+1, -z+1$; 5, $x+1, y, z$; 6, $-x+2, -y+2, -z+2$; 7, $-x+3, -y+2, -z+1$.

room temperature. A hemisphere of data (1271 frames at 5 cm detector distance) was collected using a narrow-frame method with scan widths of 0.30° in ω and an exposure time of 30 s/frame. The first 50 frames were remeasured at the end of data collection to monitor instrument and crystal stability, and the maximum correction applied to the intensities was $< 1\%$. The data were integrated using the Siemens SAINT program (11), with the intensities corrected for Lorentz factor, polarization, air absorption, and absorption due to variation in the path length through the detector faceplate. An empirical absorption correction (program SADABS) and a ψ-scan measurement were applied for **1** and **2**, respectively (12). The minimum and maximum transmission factors were 0.85 and 1.0. Additional crystallographic details are given in Table 1. For **1** the observed Laue symmetry and the systematic extinction condition ($h0l$: $h + l = 2n + 1$) were indicative of the monoclinic space groups $P2/n$ and Pn. The centrosymmetric space group $P2/n$ was assumed. A satisfactory refinement confirmed the choice of this space group.

The initial positions for all atoms were obtained using direct methods and the structures were refined by full matrix least squares techniques with the use of the SHELXTL crystallographic software package (13). For **1** the final cycle of refinement performed on F_o^2 with 2231 unique reflections afforded residuals $R_w = 0.1497$ and $R = 0.0717$ [based on

$F_o^2 > 2\sigma(F_o^2)$]. All hydrogen atoms bonded to carbon and nitrogen atoms were included in calculated positions with isotropic displacement parameters. For **2**, the final cycle of refinement performed on F_o^2 with 2992 unique reflections gave residuals $R_w = 0.0996$ and $R = 0.0467$ [based on $F_o^2 > 2\sigma(F_o^2)$]. All of the hydrogen atoms bound to carbon and nitrogen atoms were included in calculated positions with isotropic displacement parameters. The other hydrogen atoms bound to oxygen atoms were found by difference Fourier synthesis and refined isotropically. In both structures, no unusual trends were found in the goodness of fit as a function of F_o^2, $\sin\theta/\lambda$, and Miller indices. Final values of the atomic parameters and equivalent isotropic displacement parameters are given in Table 2.

Infrared spectra were recorded on a Mattson FTIR 5000 spectrometer within the range 400–4000 cm^{-1} using the KBr pellet method. Thermogravimetric analyses were carried out in air at a heating rate of 2°C/min, using a high-resolution TGA 2950 thermogravimetric analyzer (TA Instruments). Magnetic measurements were made with an Oxford Instruments Vibrating Sample Magnetometer in the temperature range 5 K $< T <$ 290 K with applied magnetic field of 1 T.

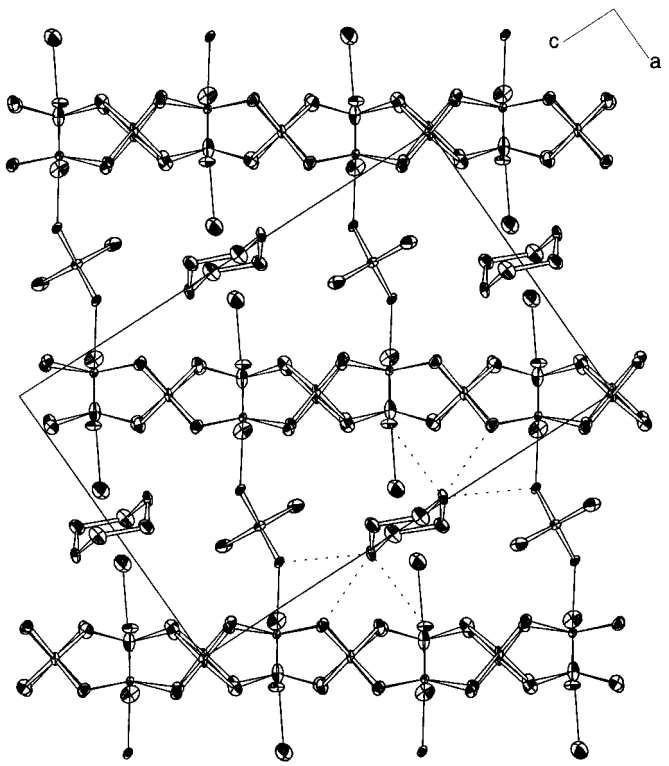

FIG. 1. View of the structure of **1** along the *b* axis showing the $[(VOPO_4)_4(H_2O)H_2PO_4]^{3-}$ framework built from$(VOPO_4)_4(H_2O)$ layers and bridging H_2PO_4 units. Hydrogen bonds are shown as dotted lines between one diprotonated piperazine cation and oxygen atoms in the $[(VOPO_4)_4(H_2O)H_2PO_4]$ framework. Hydronium ions and water molecules are omitted for clarity. Thermal ellipsoids are shown with 50% probability.

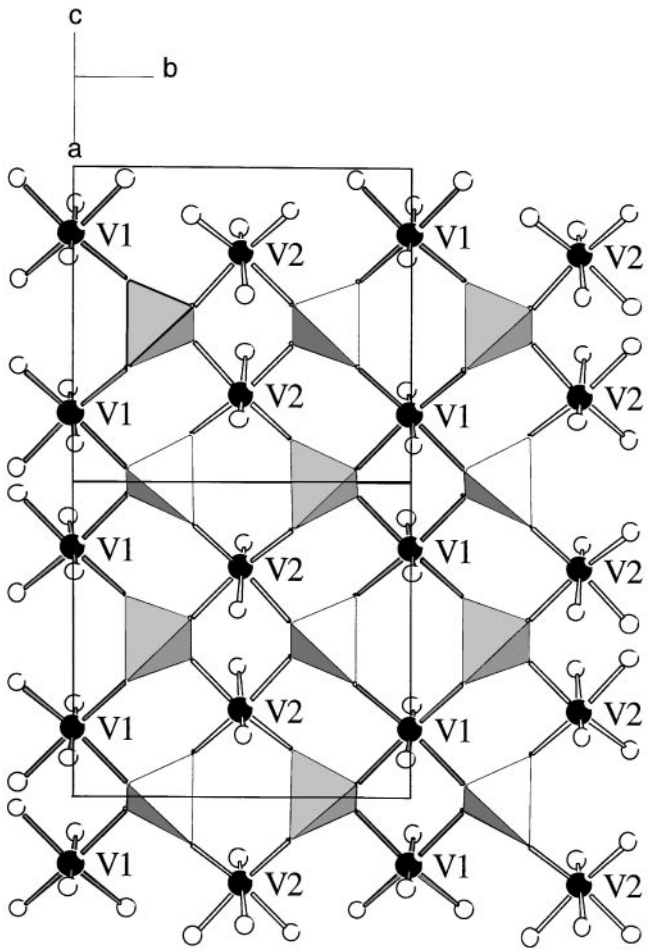

FIG. 2. View of the α-$VOPO_4$-type layer in the structure of **1** showing the ordered arrangement of $V^{IV}(1)$ and $V^{V}(2)$ atoms within each layer. PO_4 groups are shown as tetrahedra, and oxygen atoms as open circles.

RESULTS

Structure Description

Selected bond distances and angles for **1** and **2** are listed in Table 3. Compound **1** has a $[(VOPO_4)_4(H_2O)H_2PO_4]^{3-}$ framework structure that contains hydronium and diprotonated piperazine cations and water molecules (Fig. 1). The $[(VOPO_4)_4(H_2O)H_2PO_4]^{3-}$ framework is constructed by connecting $(VOPO_4)_4(H_2O)$ layers through bridging tetrahedral $PO_2(OH)_2$ groups. There are two crystallographically unique VO_6 distorted octahedra, three PO_4 tetrahedra, and one H_2PO_4 tetrahedron in the framework. Each VO_6 octahedron has one short vanadyl V=O bond (V(1)–O(9), 1.599(5) Å; V(2)–O(10), 1.583(6) Å) and four other V–O bonds intermediate in length. α-$VOPO_4$ type layers are formed by linking the VO_6 octahedra to four phosphate tetrahedra by sharing oxygen atoms. The vanadium atom

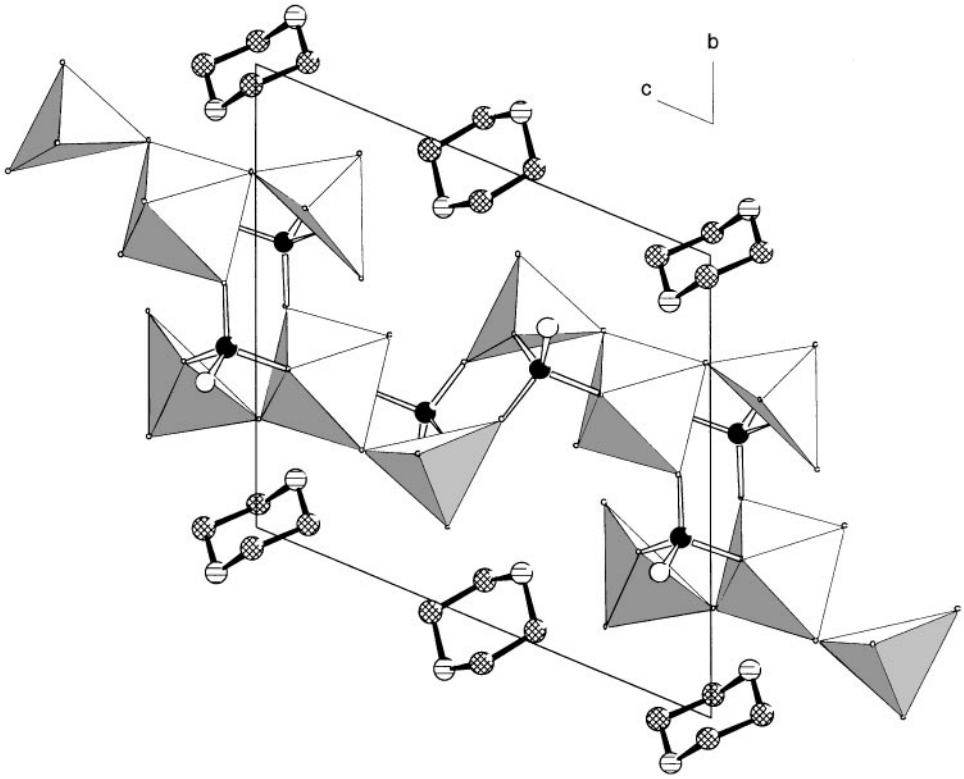

FIG. 3. View of the structure of **2** along the *a* axis showing the $[(VO)(VO_2)_2(H_2O)(PO_4)_2]$ layers in the *ac* plane. Diprotonated piperazine cations occupy interlayer sites, N and C atoms are shown as striped and hatched circles. The V–O coordination is represented by polyhedra. Thermal ellipsoids are shown with 50% probability.

coordination is completed by a long V–O distance *trans* to the V=O bond and corresponds to coordination of either a water molecule (V(2)–O(13), 2.39(1) Å) or a phosphate oxygen (V(1)–O(11), 2.191(5) Å). This arrangement results in $(VOPO_4)_4(H_2O)$ layers orientated in the (101) plane (Fig. 2) that are bridged by $H_2P(4)O_4$ units. The O(13) water molecule coordinated to the V(2) atom is disordered with half occupancy to minimize O(13)–O(13) interlayer repulsion

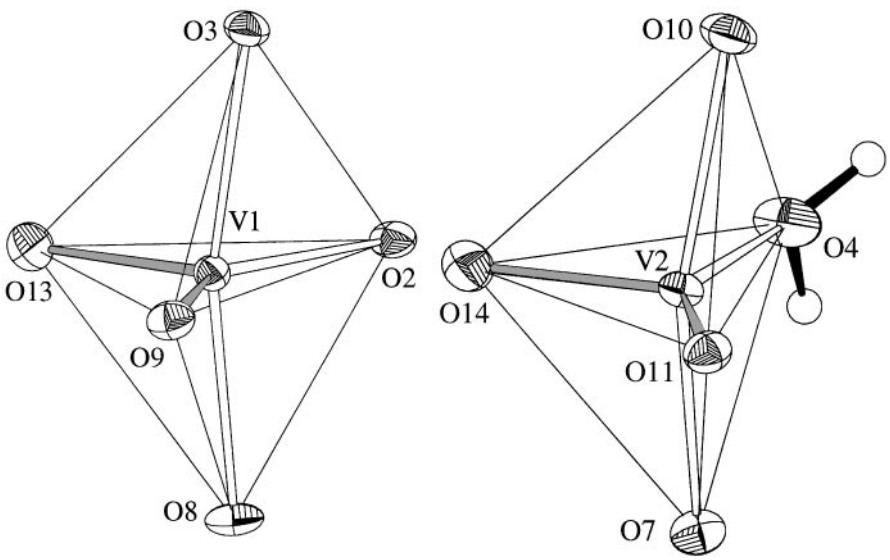

FIG. 4. Details of the V(1, 2)O_5 coordination environments in **2**. Empty bonds, V–O; filled bonds, V=O; empty circles, H atoms. Thermal ellipsoids are shown with 50% probability.

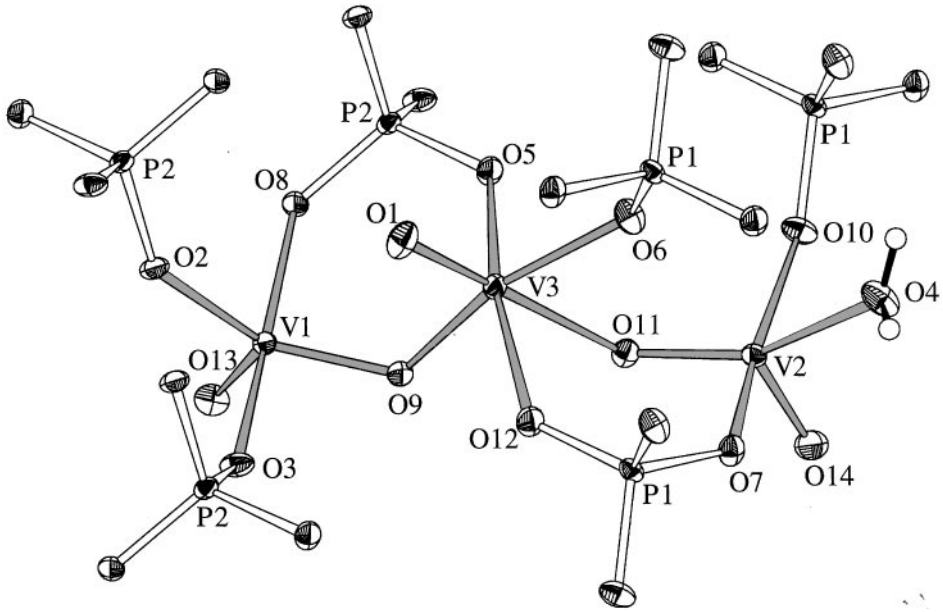

FIG. 5. The $V_3O_{13}(OH_2)$ trinuclear unit in **2** showing the connectivity of $[V^{V}–O–V^{IV}–O–V^{V}]$ and PO_4 tetrahedra. Thermal ellipsoids are shown with 50% probability.

(d[O(13)–O(13)] = 2.31 Å). The long bond lengths of the uncoordinated P(4)–O(12) bonds (1.571(6) Å) imply that they are protonated (BVS = 1.09 for O(12)) (14). Bond valence sum calculation assuming $V(1)^{IV}$–O and $V(2)^{V}$–O bonds gives BVS values of 4.07 and 5.09 indicating charge ordering. Magnetic measurement supports the BVS calculations for the V atoms (see below).

The hydrogen atoms in water molecules, hydronium, and diprotonated piperazine ions make hydrogenbonds to nearby oxygen atoms in the framework (Fig. 1). One crystallographically distinct diprotonated piperazine cation is located on an inversion center. Hydrogen bonds are formed to four adjacent oxygen atoms (O(9) and O(11)) coordinated to V(1).

The structure of **2** contains $[(VO)(VO_2)_2(H_2O)(PO_4)_2]^{2-}$ layers separated by diprotonated piperazine cations (Fig. 3). One crystallographically distinct $V^{IV}(3)O_6$ distorted octahedron, two $V^{V}(1,2)O_5$ trigonal bipyramids, and two PO_4 tetrahedra are connected by sharing oxygen atoms in each layer. The $V(1)O_5$ trigonal bipyramid has two short V=O bonds (V(1)–O(13), 1.609(3) Å; (V(1)–O(9), 1.714(3) Å) and three V–O bonds in the range of 1.899(3) Å–1.977(3) Å. The $V(2)O_5$ trigonal pyramid has also two short V=O bond distances (V(2)–O(14), 1.606(3) Å; V(2)–O(11), 1.663(3) Å) and two intermediate V–O bond distances of 1.950(3) Å and 1.952(3) Å. The longest bond distance is to a coordinated water molecule V(2)–O(4)H_2 (Fig. 4). The $V(3)O_6$ distorted octahedron has one short V=O(1) bond (1.610(3) Å). One V–O(11) bond with much longer distance (2.226(3) Å) is *trans* to V=O and the bond lengths of four other V–O bonds are in the range 1.982(3) Å–2.038(3) Å.

As Zavalij *et al.* noted, (19) five coordinated vanadium with two vanadyl oxygen atoms will normally have trigonal bipyramidal geometry. For the ideal case, the three equatorial O atoms make O–V–O angles of 120° (108.4(2), 108.8(2)°, 142.8(2)° for V(1); 104.9(2)°, 103.9(2)°, 151.2(2)° for V(2)), whereas the two apical atoms have the angle of 180° (167.0(1)° for V(1); 160.4(1)° for V(2)) (see Table 2 and Fig. 4). The V–O bond lengths fall in the range recently noted for V(V) in [2 + 3] coordination. (20)

One oxygen atom coordinated to each of the vanadium atoms, V(1)–O(13), V(2)–O(14) and V(3)–O(1), is terminal. The two other vanadyl oxygen atoms, O(9) and O(11) are shared with the $V(3)O_6$ octahedron. The three independent vanadium oxygen atom polyhedra, trigonal bipyramidal V(1) and V(2), and octahedral V(3) are connected by sharing corners to complete a mixed valence $V_3O_{13}(H_2O)$ trinuclear unit with connectivity $V^{V}(1)=O–V^{IV}(3)–O=V^{V}(2)$ (Fig. 5). Each trinuclear unit is linked by six phosphate anions to form layers of composition $[(V_3O_5)(H_2O)(PO_4)_2]^{2-}$ in the *ac*-plane as shown in Fig. 6. One diprotonated piperazine cation occupies the interlayer space. Bond valence sum calculations assuming $V(1,2)^{V}$–O and $V(3)^{IV}$–O bonds gives values of 5.02, 4.96 and 4.12, respectively (14).

The structure contains an extended network of O–H ⋯ O and N–H ⋯ O hydrogen bonds. The water molecule in the VO_4OH_2 trigonal bipyramid forms hydrogen bonds to oxygen atoms in adjacent VO_4OH_2 groups (Fig. 7). Thus, V(3)–O(5) ⋯ H_2O(4)–V(2), and H_2O(4)–V(2) ⋯ O(1)–V(3)

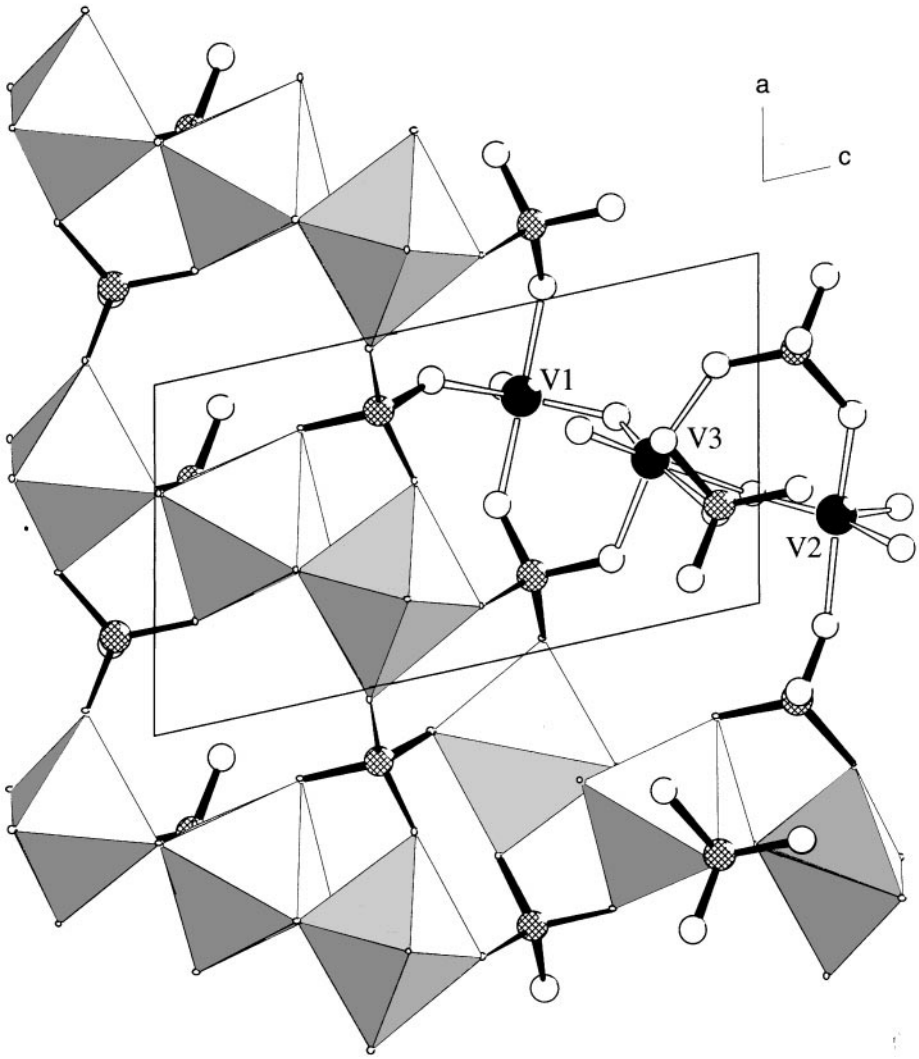

FIG. 6. $[(VO)(VO_2)_2(H_2O)(PO_4)_2]^{2-}$ layer in **2** viewed perpendicular to the *ac* plane. Filled, hatched and open circles are vanadium, phosphorus, and oxygen atoms, respectively.

bonds alternate along the *a* axis. The two H_2pipz^{2+} cations are hydrogen bonded to the oxygen atoms in the $[(VO)(VO_2)_2(H_2O)(PO_4)_2]^{2-}$ layers. Two different types of intermolecular hydrogen bonds link the H_2pipz^{2+} cations and the $[(V_3O_5)(H_2O)(PO_4)_2]^{2-}$ layer anions. The two H_2pipz cations contain two crystallographically distinct nitrogen atoms: one nitrogen atom makes hydrogen bonds with four oxygen atoms in the layers and the other with two oxygen atoms (Fig. 1).

Characterization

The infrared spectrum of **1** confirmed the presence of piperazinium cations and water molecules in the structure, as evidenced by the bands observed at 3434, 3030, 1636, 1588, 1441, 1385, and 1327 cm^{-1} (Fig. 8). Additional V=O and P–O bands are observed in the region 1300–400 cm^{-1}. The strongest bands in this region are observed at 1124, 1094, 1031, 963, 895, 671, 586, 546, and 507 cm^{-1}. The spectrum of **2** also shows characteristic absorption bands due to piperazinium cations and water (3378, 3138, 3030, 1627, 1586, 1456, and 1384 cm^{-1}) and V=O, P–O bands (1136, 1096, 1028, 994, 957, 862, 763, 598, 577, 484 cm^{-1})

Magnetic susceptibility data for **1** revealed paramagnetic behavior over the temperature range 5.4–288 K (Fig. 9). The data were fitted by using the Curie equation: $\chi_m = \chi_o + C_m/T$, $\chi_o = -1.11 \times 10^{-3}$ emu/mol and $C_m = 0.7157$ emu K/mol. The calculated effective magnetic moment μ_{eff} of 2.50 BM is in good agreement with the expected value of 2.45 BM, assuming that half the vanadium atoms in the formulae $(C_4H_{12}N_2)(H_3O)[(VOPO_4)_4(H_2O)H_2PO_4] \cdot 3H_2O$ are present as d^1 V^{IV}(1).

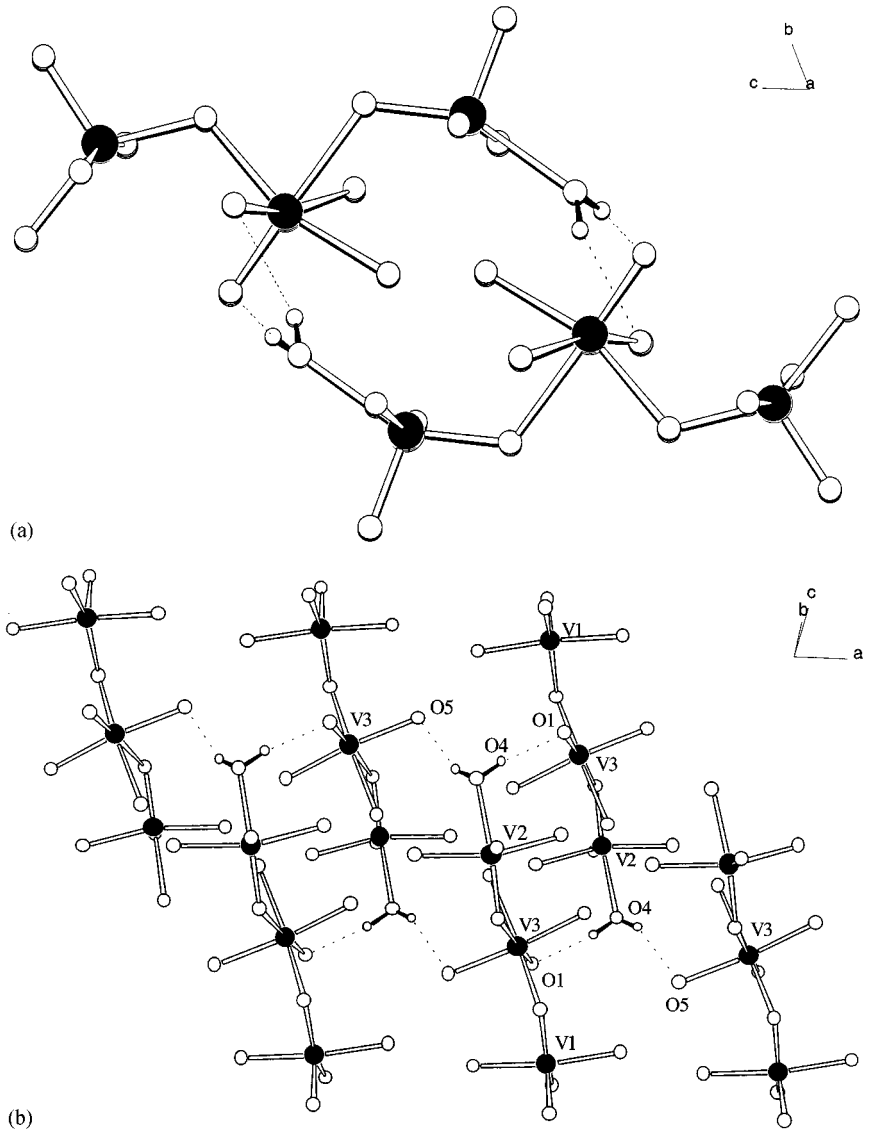

FIG. 7. Intralayer hydrogen bonds in the $[(VO)(VO_2)_2(H_2O)(PO_4)_2]$ layers viewed (a) along the *a* axis and (b) perpendicular to *ac* plane. In (b) PO_4 units are omitted for clarity.

Magnetic susceptibility data for **2** over the temperature range 4.8–290 K are shown in Fig. 9. The data were fitted by using the Curie–Weiss equation at higher temperatures ($T > 80$ K): $\chi_m = \chi_o + C_m/(T - \theta)$, $\chi_o = -9.32 \times 10^{-5}$ emu/mol, $C_m = 0.3815$ emu K/mol and $\theta = -6.55$ K. The effective magnetic moment μ_{eff} calculated from the Curie constant 1.75 BM is the value expected for an isolated $V^{IV}(3)$ ($3d^1$, $S = 1/2$, $\mu_{eff} = 1.73$ BM) in the formula $(C_4H_{12}N_2)[(VO)(VO_2)_2(H_2O)(PO_4)_2]$. The data indicate the onset of antiferromagnetic ordering at ~ 20 K.

The thermal decomposition of **1** occurs in several steps. The first step at 25– ~ 225°C corresponds to the loss of the three water molecules (weight loss: calc., 5.85%; obs., 6.04%). The evolution of piperazine and water molecules and condensation of the $PO_2(OH)_2$ group is complete at ~ 650°C (weight loss: calc., 22.20%; obs., 22.79%). At this temperature, a small weight increase is observed corresponding to the oxidation of V^{IV}. Thermogravimetric analysis of **2** shows that the evolution of piperazine and water molecules occurs in the range ~ 200–600°C in several steps. Assuming that the glassy residue corresponds to $3/2V_2O_5$ and P_2O_5, the overall observed weight loss of 21.83% is in good agreement with that calculated for the composition $(C_4H_{12}N_2)[(VO)(VO_2)_2(H_2O)(PO_4)_2]$ (21.58%).

DISCUSSION

$(C_4H_{12}N_2)(H_3O)[(VOPO_4)_4(H_2O)H_2PO_4] \cdot 3H_2O$, **1**, is a member of a family of compounds that contain $MOXO_4$ layers that are bridged by XO_4H_n groups. The structure of

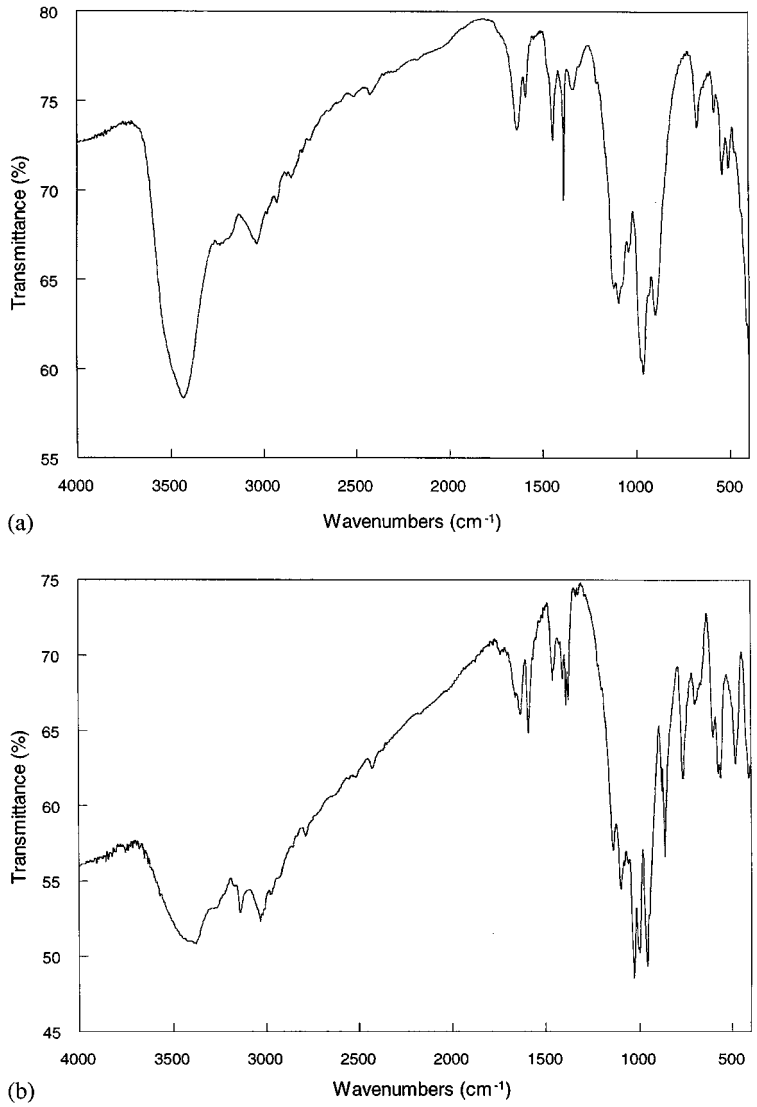

FIG. 8. Infrared spectra for **1** (a) and **2** (b).

1 is most closely related to that of $(VO)_2(PO_4)_2H_2PO_4 \cdot N_2C_2H_{10}$ (15). The $VOPO_4$ layers, each with V(IV)/V(V) = 1, have similar average in plane and interlayer dimensions (**1**, $4.438 \times 4.419 \times 7.956$ Å; $(VO)_2(PO_4)_2H_2PO_4 \cdot N_2C_2H_{10}$, $4.446 \times 4.509 \times 7.986$ Å). The mole ratios of layer to H_2PO_4 is 4:1 for **1** compared to 2:1 for $(VO)_2(PO_4)_2H_2PO_4 \cdot N_2C_2H_{10}$. In the latter, the additional bridging H_2PO_4 unit replaces the coordinated water molecules. The dissimilarities in the space filling and hydrogen bonding requirements of diprotonated piperazine and ethylenediamine cations are responsible for the structural differences.

The structure of **1** is also related to that of $Na_3VO(PO_4)(HPO_4)$ (17). In $Na_3VO(PO_4)(HPO_4)$ the HPO_4 tetrahedra do not connect the V(IV)OPO_4 layers. Each tetrahedron shares an oxygen atom with one vanadium atom to form infinite layers of composition $[VO(PO_4)(HPO_4)]^{3-}$. The layer to interlayer phosphate ratio is 1:1. The in-plane dimensions of the layers, 4.531×4.429 Å are similar to those of **1**. Mixed valence $V^{IV,\ V}O_6/PO_4$ layers are also found in the structure of $(NH_4)_{0.5}VOPO_4 \cdot H_2O$ (18).

In several V^{IV} pipz-VPOs, $[N_2C_4H_{12}]_{0.5}[VOPO_4]$, $[N_2C_4H_{12}][(VO)_4(OH)_4(PO_4)_2]$, and $[N_2C_4H_{12}]_2[(VO)_3(HPO_4)_2(PO_4)_2] \cdot H_2O$ layers structurally related to $VOPO_4$ were observed (6–8). In $[N_2C_4H_{12}]_{0.5}[VOPO_4]$ the $VOPO_4$ layers are built up from VO_5 trigonal bipyramids and PO_4 tetrahedra. In $[N_2C_4H_{12}][(VO)_4(OH)_4(PO_4)_2]$ the layers can be constructed by the insertion of $VO(OH)_2$ units into $VOPO_4$ layers at each

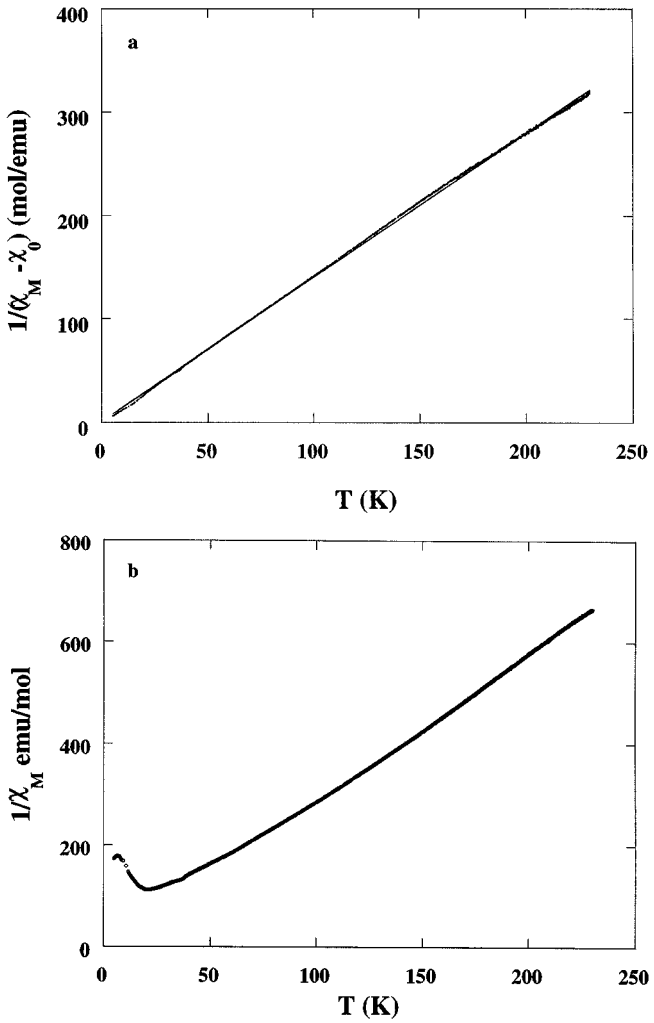

FIG. 9. Inverse molar magnetic susceptibility of **1** (a) and **2** (b) vs temperature.

vanadium site. In $[N_2C_4H_{12}]_2[(VO)_3(HPO_4)_2(PO_4)_2]\cdot H_2O$, octahedral site vacancies in $VOPO_4$ give defect layers of composition $[(VO)_3(HPO_4)_2(PO_4)_2]^{4-}$.

The coordination environments of the vanadium atoms in the structure of $(C_4H_{12}N_2)[(VO)(VO_2)_2(H_2O)(PO_4)_2]$, **2**, are unusual. Bond valence sums clearly show charge localization resulting in two V^VO_5 trigonal bipyramids and a distorted $V^{IV}O_6$ octahedron. In the related compounds $H_3N(CH_2)_3NH_3[(VO)_3(OH)_2(H_2O)_2(PO_4)_2]$ (21) and $V_3P_2O_{13}(H_2O)_2$, $H_3N(CH_2)_3NH_3$ (22), discrete trinuclear $[V_3O_{11}(OH)_2(OH_2)_2]$ corner-sharing units are also observed. The trimers are formed by one VO_5 square pyramid and two VO_6 octahedra connected to six PO_4 tetrahedra by sharing corners. $V_3P_2O_{13}(H_2O)_2$ $H_3N(CH_2)_3NH_3$ is a mixed valence compound that is better formulated as $H_3N(CH_2)_3NH_3[(VO)_3(OH)_{2-x}O_x(H_2O)_2(PO_4)_2]$, whereas $H_3N(CH_2)_3NH_3[(VO)_3(OH)_2(H_2O)_2(PO_4)_2]$ contains only V^{IV}. A range of different average oxidation states are possible for this structure type depending on synthesis conditions and the structural data indicate that the charge is delocalized over the three vanadium sites (23). The central square pyramid is connected to the octahedra through V–(OH,O)–V bonds. In contrast, in **2** charge localization occurs at a specific V^V/V^{IV} ratio and the central octahedron in the $V_3O_{13}(H_2O)$ trimer is linked to the trigonal bipyramids through V–O=V bonds (1.995 and 1.714 Å; 2.226 and 1.663 Å).

ACKNOWLEDGMENTS

This work was supported by the National Science Foundation under Grant DMR-9214804 and by the Robert A. Welch Foundation. The work made use of MRSEC/TCSUH Shared Experimental Facilities supported by the National Science Foundation under Award DMR-9632667 and the Texas Center for Superconductivity at the University of Houston.

REFERENCES

1. J. W. Johnson, D. C. Johnston, A. J. Jacobson, and J. R. Brody, *J. Am. Chem. Soc.* **106,** 8123 (1984).
2. D. Beltran-Porter, P. Amoros, R. Ibanez, E. Martinez, A. Beltran-Porter, A. Le Bail, G. Férey, and G. Villeneuve, *Solid State Ionics* **32–33,** 57 (1989).
3. P. Amoros, A. Beltran, and D. Beltran, *J. Alloys Compd.* **188,** 123 (1992).
4. K.-H. Lii, *J. Chin. Chem. Soc.* **39,** 569 (1992).
5. R. Bontchev, J. Do, and A. J. Jacobson, *Angew. Chem. Int. Ed.* **38,** 1937 (1999).
6. D. Riou and G. Férey, *Eur. J. Solid State Inorg. Chem.* **31,** 25 (1994).
7. V. Soghomonian, R. C. Haushalter, Q. Chen, and J. Zubieta, *Inorg. Chem.* **33,** 1700 (1994).
8. V. Soghomonian, Q. Chen, Y. Zhang, R. C. Haushalter, C. J. O'Connor, C. Tao, and J. Zubieta, *Inorg. Chem.* **34,** 3509 (1995).
9. V. Soghomonian, R. C. Haushalter, J. Zubieta, and C. J. O'Connor, *Inorg. Chem.* **35,** 2830 (1996).
10. X. Bu, P. Feng, and G. D. Stucky, *J. Chem. Soc. Chem. Commun.* 1337 (1995).
11. Siemens Analytical X-ray Instruments, "SAINT, Version 4.05." Madison, WI, 1995.
12. G. M. Sheldrick, "Program SADABS." University of Gottingen, 1995.
13. G. M. Sheldrick, "SHELXTL, Version 5.03." Siemens Analytical X-ray Instruments, Madison, WI, 1995.
14. N. E. Brese and M. O'Keeffe, *Acta Crystallogr. B* **47,** 192 (1991).
15. W. T. Harrison, K. Hsu, and A. J. Jacobson, *Chem. Mater.* **7,** 2004 (1995).
16. M. Tachez and F. Théobald, *Acta Crystallogr. B* **37,** 1978 (1981).
17. M. Schindler, W. Joswig, and W. H. Baur, *J. Solid State Chem.* **145,** 15 (1999).
18. J. Do, R. Bontchev, and A. J. Jacobson, *Inorg. Chem.* **39,** 3230 (2000).
19. P. Y. Zavalij and M. S. Whittingham, *Acta Crystallogr. B* **55,** 627 (1999).
20. M. Schindler, F. C. Hawthorne, and W. H. Baur, *Chem. Mater.* **12,** 1248 (2000).
21. V. Soghomonian, Q. Chen, R. C. Haushalter, J. Zubieta, C. J. O'Connor, and Y.-S. Lee, *Chem. Mater.* **5,** 1690 (1993).
22. T. Loiseau and G. Férey, *J. Solid State Chem.* **111,** 416 (1994).
23. K. Hsu, M.S. thesis, University of Houston, 1997.